JOURNAL OF GEOPHYSICAL RESEARCH, VOL. 103, NO. D16, PAGES 19,663–19,672, AUGUST 27, 1998

Raman lidar measurements of aerosol extinction and backscattering
1. Methods and comparisons

R.A. Ferrare,[1,2] S.H. Melfi,[3] D.N. Whiteman,[4] K.D. Evans,[5] and R. Leifer[6]

Abstract. This paper examines the aerosol backscattering and extinction profiles measured at night by the NASA Goddard Space Flight Center Scanning Raman Lidar (SRL) during the remote cloud sensing (RCS) intensive operations period (IOP) at the Department of Energy Atmospheric Radiation Measurement (ARM) southern Great Plains (SGP) site in April 1994. These lidar data are used to derive aerosol profiles for altitudes between 0.015 and 5 km. Since this lidar detects Raman scattering from nitrogen and oxygen molecules as well as the elastic scattering from molecules and aerosols, it measures both aerosol backscattering and extinction simultaneously. The aerosol extinction/backscattering ratio varied between approximately 30 sr and 75 sr at 351 nm. Acrosol optical thicknesses derived by integrating the lidar profiles of aerosol extinction measured at night between 0.1 and 5 km are found to be about 10–40% lower than those measured by a Sun photometer during the day. This difference is attributed to the contribution by stratospheric aerosols not included in the lidar estimates as well as to diurnal differences in aerosol properties and concentrations. Aerosol profiles close to the surface were acquired by pointing the lidar nearly horizontally. Measurements of aerosol scattering from a tower-mounted nephelometer are found to be 40% lower than lidar measurements of aerosol extinction over a wide range of relative humidities even after accounting for the difference in wavelengths. The reasons for this difference are not clear but may be due to the inability of the nephelometer to accurately measure scattering by large particles.

1. Introduction

Lidar has proven to be an effective instrument for obtaining high-resolution profiles of atmospheric aerosols. However, quantitative measurements of aerosol optical properties using a lidar system which measures only aerosol backscatter require accurate system calibration and assumptions regarding aerosol optical properties [*Klett*, 1981; *Fernald*, 1984]. Lidar systems which scan can alleviate some of these restrictions by using a multiangle integral solution of the lidar equation to solve for both aerosol backscatter and extinction [*Spinhirne et al.*, 1980; *Reagan et al.*, 1989]. However, this method requires horizontal homogeneity of the aerosols.

These restrictions are removed in the case of a combined Raman/Rayleigh-Mie lidar which measures aerosol extinction and backscattering independently [*Ansmann et al.*, 1990]. Such a Raman system, which directly measures the aerosol extinction to backscatter ratio, has been used to estimate the sizes of stratospheric aerosols following the eruption of Mount Pinatubo [*Ferrare et al.*, 1992; *Wandinger et al.*, 1995]. The NASA GSFC Scanning Raman Lidar (SRL) uses a rotating mirror to measure both horizontal and vertical profiles of aerosols and water vapor and can therefore provide very high resolution profiles near the surface. Here we show how such Raman lidar measurements can be used to ascertain properties of tropospheric aerosols and compare these measurements of aerosol optical properties with those measured by other sensors. This lidar's ability to measure aerosol extinction near the surface is especially important at night when a surface-based stable layer often forms leading to strong vertical gradients in aerosols and humidity [*Stull*, 1988]. The lidar measurements acquired near the surface can also be used to provide correlative data to assess the acrosol optical and physical measurements acquired by traditional in situ aerosol measurements.

In this first of two papers, we describe the details of the SRL, how it is used to measure aerosol backscattering and extinction, and compare these results with other instruments that directly measure aerosol optical properties. We first describe the techniques used to derive these profiles using scan data. Aerosol extinction profiles derived using the Raman nitrogen data are compared to those derived by inversion of the return signal at the laser wavelength. Profiles of the aerosol extinction/backscatter ratio derived from the Raman lidar data will also be presented. We then compare the SRL aerosol backscattering and extinction measurements with the measurements of aerosol scattering by a nephelometer and aerosol optical thicknesses derived from Sun photometers. After presenting the details of the retrieval

[1]Hughes STX, NASA Goddard Space Flight Center, Greenbelt, Maryland.
[2]Now at NASA Langley Research Center, Hampton, Virginia.
[3]Department of Physics, University of Maryland Baltimore County, Baltimore, Maryland.
[4]NASA Goddard Space Flight Center, Greenbelt, Maryland.
[5]Joint Center for Earth Systems Technology, University of Maryland Baltimore County, Baltimore, Maryland.
[6]Environmental Measurements Laboratory, Department of Energy, New York, New York.

Paper number 98JD01646.
0148-0227/98/98JD-01646$09.00

techniques and comparisons of aerosol optical properties in this paper (part 1), we show how these Raman lidar aerosol profile measurements can be used to derive other aerosol physical characteristics in a second paper, hereafter denoted by part 2. In this second paper, we shall describe and demonstrate a technique which uses a combination of the SRL measurements of aerosol extinction and backscattering with the aerosol size distributions measured on the aircraft to determine the aerosol real refractive index and single-scattering albedo [*Ferrare et al.*, this issue].

2. NASA GSFC Scanning Raman Lidar (SRL) System

The GSFC Scanning Raman Lidar employs two different lasers depending on whether data are acquired at nighttime or daytime. We discuss only nighttime measurements in this study. Descriptions of the daytime system and measurements are given by *Melfi et al.*, [1997], *Ferrare et al.*, [1997a], and *Evans et al.*, [1997]. For nighttime operations this system uses an XeF excimer laser to transmit pulses of light at 351 nm. The laser operates at 400 Hz with 30 mJ per pulse giving an average power of 12 W. Light backscattered by molecules and aerosols at the laser wavelength as well as Raman-scattered light from water vapor (402 nm), nitrogen (383 nm), and oxygen (372 nm) molecules is collected by a 0.76 m, F5.2, variable field-of-view (0.5–3.0 mrad) Dall-Kirkham telescope which is mounted horizontally on a 3.7 m optical table. The telescope is aligned with a large (1.2 m × 0.8 m) flat mirror which is also mounted on the optical table. During operations the optical table slides through an opening in the back of the trailer deploying the scan mirror that has a 180° horizon-to-horizon scan capability. Using the motorized scan mirror, atmospheric profiles can be acquired at any angle in a single plane perpendicular to the trailer or continuously scanned from horizon to horizon.

Two channels, operating in the photon counting mode, are employed for each wavelength in order to measure signals throughout the troposphere and lower stratosphere. A beamsplitter directs 5% of the return signals into the low-sensitivity channels and about 95% into the high-sensitivity channels. In normal operation, data are recorded as 1 min profiles corresponding to the accumulation of signals from about 21,000 laser shots. The photon counting data have a range resolution of 75 m. The data discussed here were acquired at night to minimize the interference from background skylight that interferes with the detection of the Raman signals, which are about 3 orders of magnitude weaker than the signal due to Rayleigh and Mie backscatter from molecules and aerosols. The entire lidar system is contained in two, environmentally controlled trailers; one trailer houses the system described above, while the second contains computers for data acquisition and analysis and the operating personnel. Several analysis programs operate in real time to monitor system performance and to provide real-time images of the evolution of both aerosols and water vapor.

3. SRL Aerosol Computations

The SRL system uses the nitrogen and oxygen Raman return signals to measure aerosol extinction. For nighttime operations using the XeF excimer laser, the outgoing wavelength is at 351 nm, while the return Raman N_2 wavelength is at 383 nm, and the return Raman O_2 wavelength is at 372 nm. Thus the total aerosol extinction coefficient measured by the lidar is actually the sum of the aerosol extinction coefficients at 351 nm and at 383 nm if the Raman nitrogen signal is used or the sum of the aerosol extinction coefficients at 351 nm and 372 nm if the Raman oxygen signal is used. If the wavelength dependence of aerosol extinction is known, the aerosol extinction cross section can be found at either of these two wavelengths. The wavelength dependence λ^{-k} between 351 nm and 383 nm is normally assumed to be unity ($k = 1$) [*Ansmann et al.*, 1990] but can vary depending on the size and composition of aerosols. Aerosol optical thicknesses measured between 340 nm and 440 nm by a CIMEL Sun photometer [*Holben et al.*, 1994; *Remer et al.*, 1997] colocated with the SRL at the Department of Energy southern Great Plains (DOE SGP) site near Lamont, Oklahoma, have shown k varies between 0 and 2. The error in the derived aerosol extinction at 351 nm using the Raman nitrogen signal is ±10% if k varies between 0 and 2 when an assumed value of $k = 1$ is used; this error reduces to (6% when the Raman oxygen signal is used because of the smaller difference between the outgoing laser wavelength and the return Raman wavelength. However, in either case, the actual errors should be smaller for the retrieved profiles discussed here since the value of k normally used in the retrievals is estimated using the wavelength dependence of aerosol optical thickness measured by the Sun photometer.

The discussion above assumes that the laser beam is fully within the field of view of the telescope so that the overlap function $O(r)$ is unity. For the SRL this occurs for ranges beyond approximately 1 km, so that when the laser beam is directed vertically, measurements of aerosol extinction are computed for altitudes above 1 km. However, by scanning the lidar system so that data are acquired at low elevation angles, the aerosol extinction coefficient profiles are derived for altitudes as low as 100 m. Figure 1a shows an example of aerosol extinction profiles measured at 0° (vertical), 70°, and 88° zenith angles as a function of altitude for 10 min integrated data acquired on the night of August 30, 1995, at Wallops Island, Virginia. A composite profile can be constructed by combining all three profiles; each profile is used for a different altitude region. For example, the 88° profile is used for altitudes between 0.1 and 0.5 km, the 70° data are used for altitudes between 0.4 and 2.0 km, while the 0° (vertical) data are used for altitudes above about 1.2 km; the profiles are linearly merged in the overlap regions.

To reduce the random error, the aerosol extinction profiles are low-pass filtered using the "nearly equal ripple" (NER) filter [*Kaiser and Reed*, 1977] using a resolution which varies with range. This filter is used to reduce the random error in the data; these random errors are computed using Poisson statistics (i.e., the standard deviation is given by the square root of the total number of photon counts.) For the aerosol extinction profiles shown in Figure 1a the resolution is 150 m for ranges beginning at 0.2 km, increases to 300 m at a range of 5 km, and to 900 m at a range of 10 km; the range resolution is varied in this manner to decrease the random error in the derived aerosol extinction. For a scan angle of 70° the corresponding altitude resolutions are 51 m for altitudes beginning at 68 m, increasing to 102 m at an altitude of 1.7 km, and to 308 m at an altitude of 3.4 km. For a scan angle of 88° the corresponding altitude resolutions are 5 m for altitudes beginning at 10 m, increasing to 10 m at an altitude of 175 m, and to 31 m at an altitude of 350 m. The range resolution of the aerosol backscatter coefficient is 75 m. For a scan angle of 70°

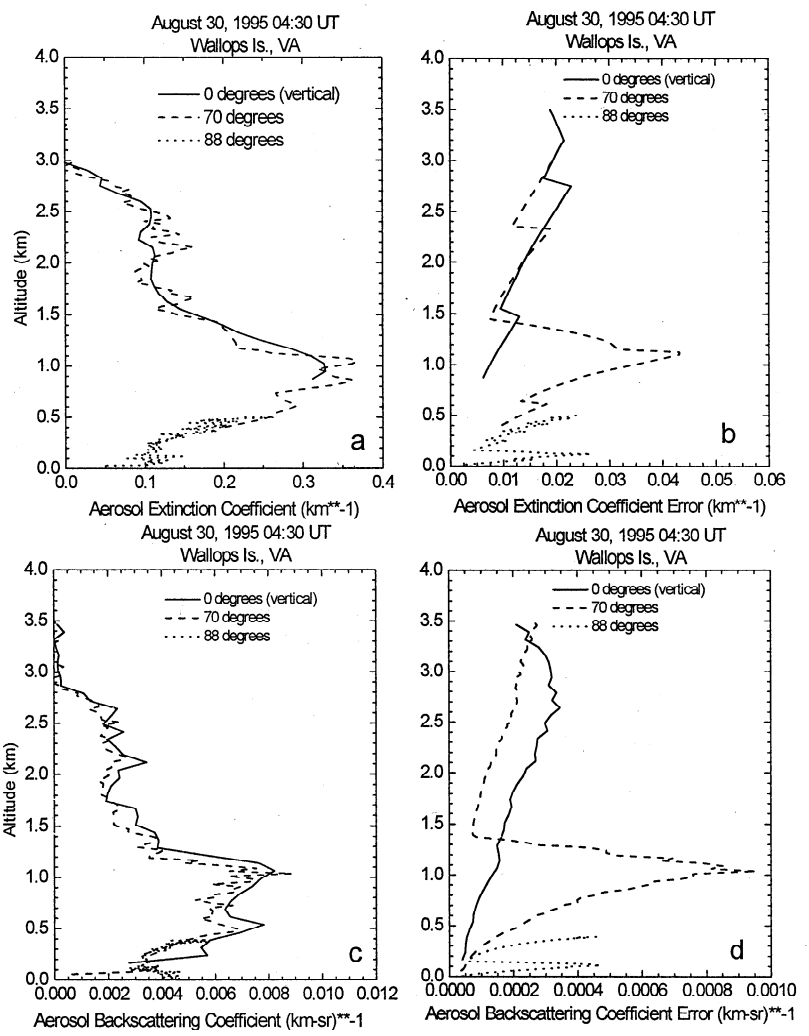

Figure 1(a). Aerosol extinction coefficient profiles derived from Scanning Raman Lidar (SRL) data on August 30, 1995. Profiles are derived at three angles (measured from zenith). (b) Random error in aerosol extinction profiles. The sharp decrease in random error is due to the transition from low to high-sensitivity channels. The periodic decrease in error is due to the change in vertical resolution. (c) and (d) Same for aerosol backscattering coefficient.

(88°), the corresponding altitude resolution is 26 (3) m. Figure 1b shows how the random error in the derived aerosol extinction profiles obtained for these various angles varies with altitude. Either integrating for a longer period and/or decreasing the range resolution can reduce the random error in the aerosol extinction profile. The low-sensitivity channels are used exclusively for ranges between 0 and about 3 km, while the high-sensitivity channels are used exclusively for ranges beyond about 4 km. Between 3 and 4 km the low- and high-sensitivity channel data are linearly merged. Converting these ranges into altitudes means that this transition from low- to high-sensitivity channels produces the abrupt decrease in random error for the 88° data at an altitude of about 120 m and a rapid decrease in random error at about 1.2 km for the 70° data.

The aerosol scattering ratio, defined as the ratio of total (molecular plus aerosol scattering) to molecular scattering and given by $\beta_m(\lambda,z) + \beta_a(\lambda,z)) / \beta_m(\lambda,z)$ is derived from the ratio of the signal detected at the laser wavelength and the Raman nitrogen signal. Since the laser beam is not fully within the field of view of the telescope for ranges less than about 1 km, a correction is applied in computing the aerosol scattering ratio to account for this overlap. This correction is obtained by placing a single, common interference filter in these two channels, so both channels observe return signals at the same wavelength. The overlap function is then computed from the ratio of the return signals in these two channels. Since both channels observe the same wavelength, this ratio does not depend on the atmospheric state. Therefore unlike the case of aerosol extinction which does not involve a ratio between two channels, application of this common filter calibration permits retrievals of aerosol scattering ratio (and consequently aerosol backscattering cross section) profiles down to the lowest range gate acquired by the lidar, which is generally 100–200 m away from the lidar. When used in conjunction with the aerosol extinction profiles described above, the aerosol scattering ratio profiles acquired at the different scan angles are merged in the same manner as are the aerosol extinction profiles described above. This is done to ensure that both scattering and extinction profiles are computed for the same location in the atmosphere.

Molecular backscattering is measured using the Raman nitrogen return at 383 nm (or the Raman oxygen signal at 371 nm) while the combined aerosol plus molecular backscattering is measured using the return signal at the laser wavelength (351 nm). Provided skies are cloud free, the lidar-derived aerosol scattering ratio is calibrated to unity at an altitude between 6 and 10 km.

This assumption is used since no appreciable variation in aerosol scattering was observed within the 5–10% random measurement error in the data in this altitude range. These results, which show a nearly constant aerosol scattering ratio in this altitude region, indicate that aerosol scattering (at 351 nm) is negligible so that errors in the scattering ratio and backscattering cross section associated with this assumption should be at most 5–10%. If we assume a worst-case error of 10% in the aerosol scattering ratio, the resulting error in the aerosol backscattering cross section is about 0.0008 km^{-1} at the surface and 0.0005 km^{-1} at an altitude of 4 km.

A correction is computed to account for the difference in atmospheric transmission between the return signal at the laser wavelength and the Raman nitrogen (or oxygen) return signal. The difference in atmospheric transmission between the two wavelengths, which is due predominantly to the λ^{-4} wavelength dependence of molecular scattering, is derived by computing molecular scattering from the radiosonde density data and aerosol extinction from the lidar data. When computed using the Raman nitrogen signal, this correction, which increases with range away from the lidar, is less than 20% for altitudes below 10 km. When Rayleigh scattering is computed using the radiosonde density profile, and aerosol extinction is derived from the lidar Raman N_2 return, this correction can be computed to within 1–2%. For scan data acquired at low-elevation angles under hazy conditions, this correction increases to about 30–50%; under these conditions the uncertainty in the correction depends heavily on the wavelength dependence of aerosol extinction. For the case described above where the wavelength dependence λ^{-k} between 351 nm and 383 nm varies between $k = 0$ and 2 from an assumed value of $k = 1$, the uncertainty in this differential atmospheric transmission terms increases to 20–25%. In these cases, the Raman oxygen signal is used instead of the Raman nitrogen signal since the smaller difference between the two wavelengths (i.e., 351 (laser)-372 nm (Raman O_2) versus 351 (laser)-383 nm (Raman N_2)) reduces the uncertainty in the differential atmospheric transmission term. For vertical data, the correction reduces to about 12% at an altitude of 10 km, while for scan data acquired at low-elevation angles under hazy conditions, this correction increases to about 15–30%; the errors in these values due to uncertainties in the wavelength dependence of aerosol extinction are 1% (vertical) and 10% (horizontal). Thus using the Raman oxygen signal instead of the Raman nitrogen signal reduces the differential atmospheric correction (and uncertainties) by about a factor of 2.

When using the Raman oxygen signal and/or nitrogen signal in computing aerosol extinction, the uncertainty in the differential atmospheric transmission correction must be weighed against the random error in the data. Recall that the random error in the lidar signal is computed using Poisson statistics, so the standard deviation is given by the square root of the number of photon counts. Although the Raman scattering cross section for oxygen is about 30% greater than the Raman nitrogen scattering cross section, the nitrogen molecule density is over 3 times larger than the oxygen molecule density for altitudes below about 100 km. This means that the random error in the aerosol extinction coefficient is about 50% smaller when the Raman nitrogen signal is used to derive aerosol extinction. Therefore when the uncertainty in the differential atmospheric correction is less than a few percent, as in the case of vertically pointing data, the Raman nitrogen signal is used to derive aerosol extinction. For scan data acquired during hazy conditions, aerosol extinction is computed using the Raman oxygen signal to minimize the error in the differential transmission correction at the expense of higher random noise.

When used in conjunction with the aerosol extinction profiles described above, the aerosol scattering ratio profiles acquired at the different scan angles are merged in the same manner as are the aerosol extinction profiles described above. This is done to ensure that both scattering and extinction profiles are computed for the same location in the atmosphere. The profile of the aerosol backscattering cross section is then computed from the profile of the scattering ratio discussed above and from the molecular

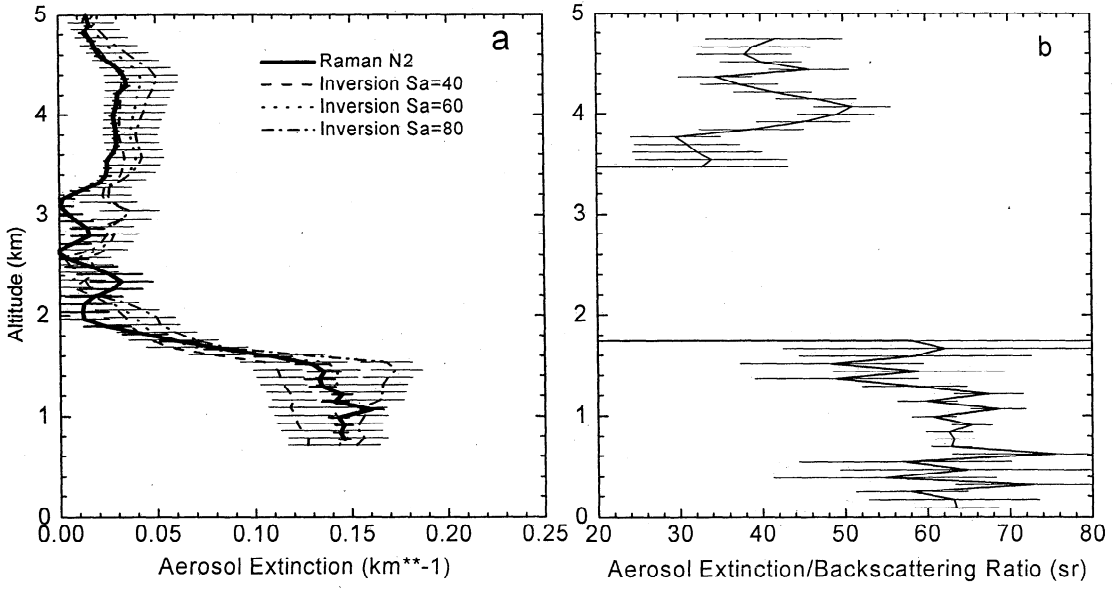

Figure 2(a). Aerosol extinction coefficient profiles derived using the Raman nitrogen data as well as by inverting the return data at the laser wavelength. These data were acquired between 0430 and 0530 UT on April 21, 1994. The inversion profiles are derived using three extinction/backscattering ratio (S_a) values. (b) Aerosol extinction/backscattering ratio profile derived from the Raman lidar data for the same night. S_a is not derived between 1.9 and 3.5 km due to low values of aerosol extinction.

backscattering cross section. The molecular backscattering cross section is obtained from the molecular density profile that is computed from coincident radiosonde pressure and temperature data. Profiles of the aerosol extinction/backscatter ratio are then computed from the extinction and backscattering profiles.

The maximum range depends primarily on the amount of data integrated, the vertical resolution, and the scan angle. Figure 1c shows the derived aerosol backscattering profiles corresponding to the aerosol extinction profiles in Figure 1a, while Figure 1d shows the corresponding errors in these profiles. For the nominal 1 min, 75 m resolution, vertical profiles, the random error is less than about 10% below 15 km. Since atmospheric attenuation increases near the surface (especially under hazy conditions), these maximum ranges decrease to about 8–10 km (or equivalently, altitudes of 300–400 m) for low elevation angles.

A comparison of the aerosol extinction profiles measured using only the return signal at the laser wavelength and the Raman technique is shown in Figure 2a. Figure 2a shows the aerosol extinction derived from the SRL Raman nitrogen data acquired while pointing vertically on the night of April 21, 1994, at the SGP site near Lamont, Oklahoma. Figure 2b shows the corresponding profile of the aerosol extinction/backscatter ratio S_a measured by the Raman lidar. Note that S_a is approximately 60 sr within the lowest 1.5 km and decreases to around 40 sr in the elevated aerosol layer between 3.5 and 4.5 km. Because the aerosol extinction coefficient computed from the Raman nitrogen data was generally below 0.02 km^{-1} between 1.8 and 3.2 km and is therefore comparable to the size of the random error in the derived aerosol extinction, S_a was not computed in this altitude range. This variation of S_a with altitude, which indicates that the aerosol size and/or composition varied between the two layers, is examined in greater detail in the companion paper part 2.

Aerosol extinction profiles derived by inverting only the Rayleigh/Mie return signal at 351 nm using various values of S_a are also shown in Figure 2a. These inversions are computed using the method described by *Fernald* [1984]. Using a value of $S_a = 60$ sr within the lowest 0–1.6 km produces an aerosol extinction profile which most closely matches the extinction profile derived from the Raman nitrogen channel data; in the upper layer a value of $S_a = 40$ sr is required. Thus using a single value of S_a throughout this entire altitude region would result in an erroneous aerosol extinction profile. In addition, the results also demonstrate that for simple nonscanning lidar systems, aerosol extinction profiles derived by inverting the Rayleigh/Mie signal at the laser wavelength without additional information to specify S_a are meaningless.

4. Experimental Data

The lidar data discussed here were acquired during the remote cloud sensing (RCS) intensive operations period (IOP) held at the Department of Energy (DOE) southern Great Plains (SGP) cloud and radiation testbed (CART) site near Lamont, Oklahoma, in April 1994. During the RCS IOP the lidar acquired a total of 74 hours of data over nine nights operating in the scan mode. An additional 49 hours of data were acquired over six nights when only vertical profiles were acquired. The lidar was oriented so that scan data were acquired adjacent to a 60 m instrumented tower that was located approximately 300 m away from the lidar. A Radiance Research Corporation integrating nephelometer model 903 [*Leifer et al.*, 1995a, b] measured the aerosol scattering coefficient (530 nm) near the top of this tower during three of the nights the lidar acquired data in the scan mode. Radiosondes carrying Vaisala radiosondes were launched at this site approximately 50 m away from the lidar every 3 hours throughout the entire experiment. In addition, an Atmospheric Emitted Radiance Interferometer (AERI) [*Smith et al.*, 1995] was also located at this site. Radiances measured by this instrument were used to derive temperature and moisture profiles every 10 min throughout the lowest few kilometers during the experiment [*Knuteson et al.*, 1996]. Temperature profiles measured by both the radiosondes and those derived from the AERI radiances are used in the analysis of the lidar data. During two nights of lidar operations, the University of North Dakota Citation aircraft flew above the CART site and measured water vapor and the aerosol size distribution. These aerosol size distribution measurements are discussed in detail in part 2.

A CIMEL multiband automatic Sun- and sky-scanning radiometer [*Holben et al.*, 1994] was also deployed at this site and acquired aerosol and water vapor data throughout this experiment. During the RCS IOP this instrument used six interference filters at 339, 380, 441, 672, 873, and 1022 nm to acquire aerosol measurements during daytime, cloud-free conditions. Aerosol optical thickness, phase function, size distribution, and integrated water vapor were derived from a combination of Sun and sky brightness measurements measured by this instrument. The aerosol optical thickness calibration for this Sun photometer was obtained from an intercomparison with a standard reference Sun photometer at Goddard Space Flight Center. This reference instrument was calibrated using a series of spectral measurements at various air masses (i.e., "Langley plot") using data acquired at the top of Mauna Loa, Hawaii. The total error in the field instrument calibration is the uncertainty associated with the transfer of the calibration from the reference instrument plus the error in the reference instrument defined from the Mauna Loa calibration. The resulting total error in the aerosol optical thickness at 340 nm is about 0.02 [*Holben et al.*, 1998].

5. SRL Aerosol Comparisons

5.1. Aerosol Optical Thickness

During the RCS IOP, there were nine nights when measurements were acquired at slant scan angles as well as vertical measurements so that aerosol extinction profiles for altitudes less than 0.8–1 km could be derived using either the Raman nitrogen or the oxygen signal. Figure 3a shows the aerosol optical thickness derived from the lidar aerosol extinction profiles on these nights as well as the aerosol optical thicknesses derived from the CIMEL Sun photometer measurements at 340 nm on cloud-free days. For these measurements the SRL aerosol optical thickness is computed by integrating the aerosol extinction coefficient for altitudes between 0.015 and 5.0 km and so does not account for aerosols above 5 km. The estimated aerosol optical thickness at 351 nm due to stratospheric aerosols is 0.04 during April 1994 [*Jager et al.*, 1997].

Water vapor mixing ratio profiles are computed using the SRL data acquired during the RCS IOP following the methods described by *Ferrare et al.* [1995]. The water vapor mixing ratio profiles are then integrated with altitude to compute the

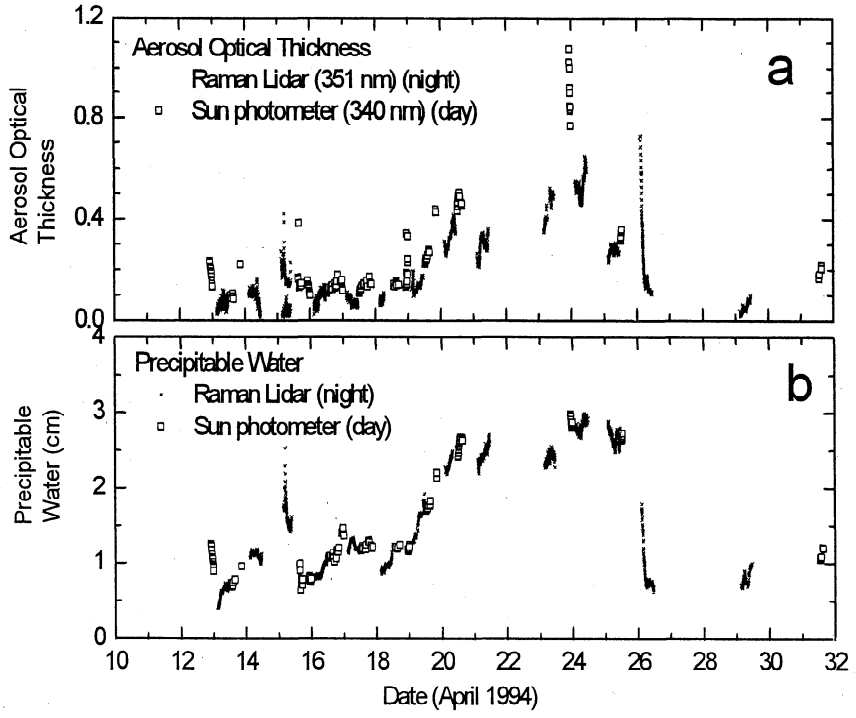

Figure 3(a). Aerosol optical thickness measured by the SRL at 351 nm during the night and the CIMEL Sun photometer at 340 nm during the day during the remote cloud sensing (RCS) intensive operations period (IOP) in April 1994. Lidar values are for aerosol optical thickness between 0.015 and 5 km. (b) Same except for precipitable water vapor. Lidar values are for altitudes between 0.015 and 8 km.

precipitable water amounts shown in Figure 3b. The lidar measurements of precipitable water are derived by integrating the water vapor mixing ratios between the altitudes of 0.015 and 8 km. Also shown in Figure 3b are the precipitable water estimates derived from the CIMEL Sun photometer. These values were derived using the solar radiances measured at 940 nm as discussed by *Halthore et al.* [1996]. This figure shows that the increase in aerosol optical thickness measured by the SRL and the Sun photometer after April 18 shown in Figure 3a was accompanied by an increase in precipitable water.

Although the measurements from the SRL and Sun photometer cannot be compared directly, the optical thicknesses derived from both systems show the same trends in aerosols and are interconnected. Note the increase in aerosol optical thickness shown by both systems between April 18 and 21. The rapid decrease in aerosol optical thickness and water vapor shown by the SRL data on the night of April 15 was associated with the passage of a cold front over the SGP site. B. B. Demoz et al. (manuscript in preparation, 1997) discuss how the complex interactions of a cold front and dry line led to these lidar observations. Similarly, the rapid decrease of aerosol optical thickness and water vapor on the night of April 26 was associated with the passage of the dry line late on April 25. Strong storms and high winds accompanied the passage of this dry line. The lack of Sun photometer measurements after April 21 was due to the presence of clouds.

The values of aerosol optical thickness computed in this manner for the nights of April 16,17, and 18 are 10–40% lower than those measured by the CIMEL Sun photometer during the daytime measurements. This difference may be due to (1) the additional aerosol optical thickness above 5 km produced by stratospheric aerosols, (2) the 165 m lower limit of the aerosol extinction profiles computed using the aerosol backscattering coefficient and the estimated aerosol extinction/backscattering ratio (see next paragraph), (3) diurnal differences in both the aerosol amounts and the properties, and (4) uncertainty in the Sun photometer measurements. The diurnal differences may also explain the large aerosol optical thicknesses measured by the Sun photometer on April 23. During the daytime, with constant mixing ratio and decreasing temperatures with altitude in the boundary layer, the relative humidity can increase to values well above 80–90%; this increase in relative humidity leads to hygroscopic growth of the aerosol particles, thereby increasing the optical extinction.

On six nights during the RCS IOP the lidar acquired only vertical data, so aerosol extinction could not be computed using the Raman channels below about 0.8 km. Therefore the aerosol backscattering coefficient derived from the lidar data is used to estimate aerosol extinction and aerosol optical thickness. The aerosol scattering ratio is first computed from vertical data for altitudes above 165 m and then used to compute the aerosol backscattering coefficient. Vertical profiles of aerosol extinction are computed from these profiles of the aerosol backscattering coefficient using an estimate of the aerosol extinction/backscattering ratio. The values of the aerosol extinction/backscatter ratio are computed from the lidar measurements of aerosol extinction and backscattering made on the nights when slant path measurements were acquired. Note that a value of $S_a = 40$ sr is used for the April 13–18 computations of aerosol extinction which were used to compute the aerosol optical thicknesses for this period shown in Figure 3a.

Figure 4 shows how the aerosol extinction/backscattering ratio derived from SRL data varied with time throughout the experiment. These profiles represent averages for each of the nights of observations; error bars represent the standard deviations of the measurements. A worst-case uncertainty in the aerosol-scattering

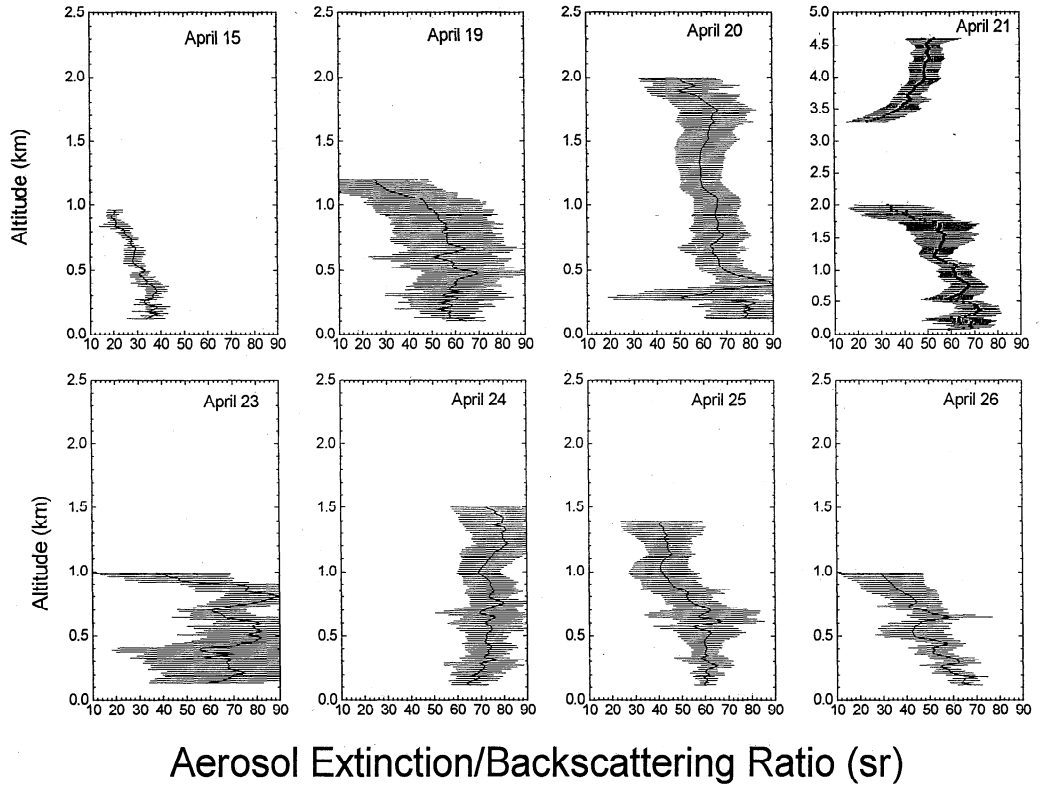

Figure 4. Profiles of aerosol extinction/backscattering ratio S_a measured by the SRL during the RCS IOP in April 1994.

ratio calibration of 10% produces an error in S_a of about 12–15%. Aerosol extinction/backscattering values are shown for these altitude regions where the aerosol extinction value was greater than 0.02 km^{-1}. S_a varied between values of 20 sr on April 15 to approximately 80 sr on April 24. As the aerosol extinction and aerosol optical thickness increased after April 18, as shown in Figure 3, S_a also increased, as shown in Figure 4. This increase in S_a indicates that the aerosol characteristics as well as aerosol concentrations varied during this period. The decrease in S_a from approximately 62 sr near the surface to about 40 sr between 3.5 and 4.5 km on April 21 also shows that aerosol characteristics varied with altitude as well. This variation in aerosol characteristics will be described in greater detail in a companion paper part 2.

The variability in S_a observed by the Raman lidar, caused by the variation in aerosol physical properties (i.e., size, shape, and composition), has been observed elsewhere. *Ansmann et al.* [1992] used a Raman lidar operating at 308 nm to obtain an extinction to backscatter ratio profile for the cloud-free lower troposphere over northern Germany; this profile had an average value of about 33 sr independent of range between 1.3 and 3.0 km. *Takamura and Sasano* [1990] used a combination of aerosol backscatter lidar, aerosol counter, and Sun photometer measurements to measure S_a and found values ranging between 32 and 66 sr at a wavelength of 532 nm. *Takamura et al.* [1994] used a similar combination of measurements to measure S_a over southern Japan; values ranged between 20 and 70 sr. *Rosen et al.* [1997] used simultaneous surface measurements of extinction by a nephelometer and backscattering by a backscattersonde to measure the extinction/backscattering ratio of aerosols over the southwestern United States and found values of S_a of 41 ±8 sr at 490 nm and 30 ±6 sr at 700 nm. These results indicate that a "universal" value of S_a does not exist. In a companion paper part 2, we show that the S_a values measured by the SRL are, in general, consistent with those computed using Mie theory using the aerosol size distributions measured during the lidar observations.

5.2. Comparison With Nephelometer Measurements

During the RCS IOP the DOE Environmental Measurements Laboratory (EML) operated an aerosol measurement package on the top of the 60 m tower located at the CART site [*Leifer et al.*, 1995a, b]. Included in this package was a Radiance Research Corporation integrating nephelometer model 903 (530 nm) which provided 15 min averaged measurements of the aerosol-scattering coefficient. This nephelometer has a small scattering volume with rapid exchange rate and so is designed to measure aerosol scattering with minimal heating (< 1°C) to minimize drying of the aerosol (R. Weiss, personal communication, 1998). On three nights the nephelometer measured aerosol scattering, while the SRL collected scan angle data alternating between zenith angles of 0°, 80°, and 85°. The lidar measurements at 80° zenith angle were oriented to scan directly alongside these aerosol sensors mounted at the top of the tower approximately 300 m away. Figure 5 shows a comparison of the aerosol scattering coefficient (530 nm) measured by the nephelometer (right axes) and the aerosol extinction coefficient (351 nm) measured by the SRL (left axes). Note that both instruments show good agreement in measuring trends of either increasing or decreasing amounts of aerosols. In comparing these results, recall that the SRL measurements correspond to a 75 m long range bin, while the nephelometer measurements represent point measurements.

The lidar aerosol extinction coefficients shown in Figure 5 are computed from the lidar data in two ways. The first method uses

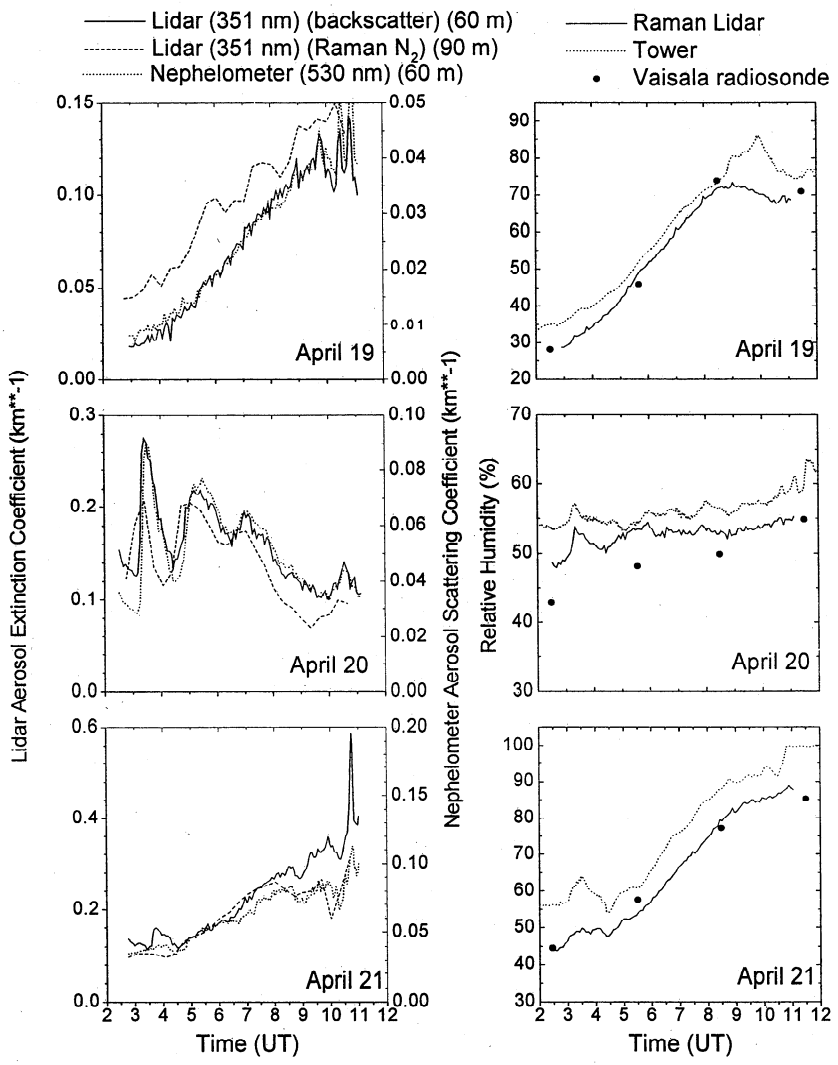

Figure 5. (left) Comparisons of the aerosol extinction coefficient measured by the lidar (left axes) at 351 nm with the aerosol scattering coefficient measured by an integrating nephelometer (right axes) at 530 nm mounted on the 60 m tower at the southern Great Plains (SGP) site during the RCS IOP. The lidar values are computed using two different methods: the first uses the aerosol backscattering coefficient and the derived extinction/backscattering ratio; the second uses the Raman N_2 return signal at 90 m. (right) Relative humidity measured by the lidar, tower hygrometer, and radiosondes at an altitude of 60 m on these same nights.

the lidar measurements of the aerosol backscattering coefficient and the value of the aerosol extinction/backscattering ratio to compute aerosol extinction. The values $S_a = 60$ (April 19), $S_a = 80$ (April 20), and $S_a = 70$ (April 21), shown in Figure 4 are used to convert the aerosol backscattering coefficients to the aerosol extinction coefficients shown in Figure 5. In the second method, the aerosol extinction coefficient measured directly using the Raman nitrogen return signal is used. However, since aerosol extinction cannot be directly measured within about 1 km of the lidar in the overlap region, the lowest altitude for direct aerosol measurements at the 85° scan angle is about 90 m; in addition, at this altitude and scan angle the measurement is about 700 m away from the tower. Figure 5 also shows these lidar aerosol extinction measurements derived from the Raman channel on these nights. These measurements showed that on April 20 and 21, aerosol extinction derived from the lidar measurements using both methods agreed very well. On April 19, aerosol extinction derived from the Raman channel was greater than that derived using the aerosol backscattering and the estimated S_a value. These two values of aerosol extinction may differ because of variations in aerosol amounts and properties with altitude and/or an incorrect value of the extinction/backscattering ratio.

Figure 5 also shows the nephelometer measurements of aerosol scattering coefficient for the three nights. These comparisons show that the aerosol extinction coefficients measured by the lidar are a factor of about 3 greater than the aerosol scattering coefficients measured by the integrating nephelometer. This difference can be partially explained by the wavelength difference of the two measurements. The wavelength dependence of aerosol optical thickness measured by the Sun photometer during these days shows that the aerosol optical thickness at 351 nm should be about 1.8 times that at 530 nm. Although this reduces the difference between the aerosol extinction coefficient between the two measurements, the nephelometer values are still about 40% below the lidar values. Since the lidar measurements are of aerosol extinction, while the nephelometer are of aerosol scattering, aerosol absorption may account for some of the remaining differences. However, for most aerosols, aerosol absorption should be less than 10–15% [*Waggoner et al.*, 1981; *d'Almeida et al.*, 1991], so aerosol absorption cannot account for this entire difference.

The reasons for these differences are not clear at this time. We do not feel that this difference was due to miscalibration of the ARM nephelometer. After the experiment, this nephelometer was compared with a TSI integrating nephelometer, which was later installed at the SGP site. These nephelometers compared to within a few percent. One reason for the lidar/nephelometer difference may be the loss of particles in the nephelometer inlet, which would reduce the measured scattering coefficients. Another possible reason for this difference may be that the nephelometer dries the aerosols; this would cause the relative humidity to be less than ambient and decrease the measured scattering coefficient. When comparing aerosol trends observed by nephelometers and particle sizes measured by a forward scattering spectrometer probe (FSSP) counter during aircraft flights over England, *Kilsby and Smith* [1987] found that nephelometers failed to read high scattering coefficients during periods of high relative humidity. The relative humidities measured by the tower hygrometer, the SRL, and Vaisala radiosondes also at an altitude of 60 m are also shown in Figure 5. The relative humidity measured at this level on April 19 increased from about 30% to about 80%; on April 21 the humidity increased from 55% to 85%. However, since on both nights the ratio of aerosol extinction derived from the lidar measurements to those derived from the nephelometer, as shown in Figure 5, remained nearly constant, it does not appear that this mechanism can explain the differences.

Another potential cause for the underestimate by the nephelometer may be because the nephelometer does not measure over the entire range of scattering angles but rather over the range between 7°–170° [*Cheng*, 1996]. *Heintzenberg and Charlson* [1996] report that studies have found that such truncation errors due to neglecting forward scattering by aerosols range from 10 to 20% for realistic aerosol size distributions. *Anderson et al.* [1996] found that such nephelometer restrictions can lead to errors of 10% for typical accumulation mode aerosols (volume mean diameters between 0.2 and 0.4 μm) but increase to 20–50% for coarse mode particles (diameter greater than 1 μm).

Indirect comparisons of the aerosol optical thickness estimated by integrating the nephelometer values with altitude have found similar underestimates from nephelometer measurements. *Kaufman et al.* [1986] found that the aerosol optical thicknesses derived from an airborne nephelometer measurements were a factor of 2 smaller than those derived from simultaneous Sun photometer measurements; in this comparison an attempt was made to correct the nephelometer measurements for hygroscopic growth of the aerosol particles. Similarly, *Bergin et al.* [1996] compared aerosol optical thicknesses derived from the multifilter rotating shadowband radiometer (MFRSR) downwelling and diffuse radiance measurements and those derived from the nephelometer mounted on the tower during the April 1994 RCS IOP. The aerosol optical thicknesses derived from the nephelometer values were found to be about a factor of 4 smaller than those derived from the MFRSR data. Since these nephelometer measurements were used to estimate the aerosol burden throughout the boundary layer, the authors attributed some of this difference to nonuniform distribution of aerosols as well as to light scattering by particles greater than 1 μm.

We feel that the difference between the lidar aerosol extinction and the nephelometer aerosol scattering measurements is most likely due to (1) the limitations of the nephelometer in measuring forward scattering produced by large particles and (2) aerosol absorption. However, without additional information it is difficult to specifically determine how these mechanisms produced the observed differences.

6. Conclusion

By measuring Raman scattering from nitrogen as well as the Rayleigh/Mie scattering from molecules and aerosols at the laser wavelength, the NASA GSFC Scanning Raman Lidar measures both aerosol backscattering and extinction directly and simultaneously. The Raman technique measures aerosol extinction and backscattering directly and therefore does not require assumptions regarding the relationship between aerosol extinction and backscattering or assumptions regarding the aerosol distributions. Since the Raman technique actually measures the sum of the aerosol extinction coefficients at two wavelengths, some estimate of the wavelength dependence of aerosol extinction is desired to reduce the 5–10% error which can be introduced if the assumed wavelength dependence is incorrect. In the present case, the wavelength dependence is determined from Sun photometer measurements of aerosol optical thickness. The Raman technique also requires measurements of atmospheric density which, in the studies described here, are computed from pressure and temperature profiles measured by radiosondes.

The SRL aerosol backscattering and extinction measurements acquired during the RCS IOP experiment which occurred during April 1994 at the Department of Energy southern Great Plains site are compared with the aerosol scattering measured by a tower-mounted integrating nephelometer and the aerosol optical thickness measurements derived from a Sun photometer. Even after accounting for the difference in wavelength between the instruments (SRL 351 nm versus nephelometer 530 nm), the nephelometer measurements of aerosol scattering are about 40% lower than the values of aerosol extinction derived from the lidar measurements. These differences do not appear to be related to variations in relative humidity. The reason for this underestimate of scattering by the nephelometer is not known but may be due to the inability of the nephelometer to accurately measure scattering by large particles within scattering angles between 0° and 7° [*Heintzenberg and Charlson*, 1996; *Anderson et al.*, 1996]. This difference between the lidar measurements of aerosol extinction and the nephelometer measurements of aerosol scattering could be examined in more detail if detailed measurements of the aerosol size distribution were available. Such measurements could be used to determine the contribution made by large particles to the total scattering measured by the nephelometer.

Aerosol optical thicknesses are derived by integrating the lidar profiles of aerosol extinction between 0.1 and 5 km. The lidar measurements of aerosol optical thickness, which were acquired at night, are about 10–40% lower than aerosol optical thicknesses measured by a Sun photometer during the day. This difference is most likely due to stratospheric aerosols which produced an aerosol optical thickness of about 0.04 during April 1994 at this latitude [*Jager et al.*, 1997] as well as diurnal differences in aerosol properties and concentrations.

The retrieval of aerosol extinction and backscattering profiles, as well as aerosol optical thickness, during daytime operations is under development. The GSFC Scanning Raman Lidar has been modified to acquire both daytime and nighttime measurements of aerosols and water vapor [*Melfi et al.*, 1997; *Ferrare et al.*, 1997, *Evans et al.*, 1997]. In addition, the Raman lidar at the Department of Energy southern Great Plains cloud and radiation testbed (CART) site has recently demonstrated its ability to measure water vapor and aerosol profiles during both daytime and nighttime operations [*Goldsmith et al.*, 1996]. Measurements from these systems will be used to evaluate the aerosol measurements acquired by ground-based and satellite remote

sensing systems as well as to study the diurnal behavior of aerosols and water vapor.

References

Anderson, T.L., et al., Performance characteristics of a high sensitivity, three-wavelength, total scatter/backscatter nephelometer, *J. Atmos. Oceanic Technol., 13*, 967–986, 1996.

Ansmann, A., M. Riebesell, and C. Weitkamp, Measurement of atmospheric aerosol extinction profiles with a Raman lidar, *Opt. Lett., 15*, 746–748, 1990.

Ansmann, A., M. Riebesell, U. Wandinger, C. Weitkamp, E. Voss, W. Lahmann, and W. Michaelis, Combined Raman elastic-backscatter lidar for vertical profiling of moisture, aerosol extinction, backscatter, and lidar ratio, *Appl. Phys. Ser. B., 55*, 18–28, 1992.

Bergin, M.H., J.A. Ogren, R.N. Halthore, S.E. Schwartz, and S. Nemesure, Aerosol optical depth estimates based on nephelometer measurements at the atmospheric radiation measurement program southern Great Plains site, paper presented at the Sixth Atmospheric Radiation Measurement Program Science Team Meeting, Department of Energy, San Antonio, Tex., March 1996.

Cheng, M.D., ARM Aerosol Observing System and its measurements, paper presented at the Second ARM Aerosol Workshop, Department of Energy, Oakridge National Laboratory, Tenn., November 1996.

d'Almeida, G.A., P. Koepke, and E.P. Shettle, *Atmospheric Aerosols: Global Climatology and Radiative Characteristics*, 559 pp., A. Deepak, Hampton, Va., 1991.

Evans, K.D, S.H. Melfi, R.A. Ferrare, G. Schwemmer, and D.N. Whiteman, First daytime observations of the GSFC Scanning Raman Lidar (abstract), *EoS Trans. AGU, 78*(17), S78, 1997.

Fernald, F.G., Analysis of atmospheric lidar observations: Some comments, *Appl. Opt., 23*, 652–653, 1984.

Ferrare, R.A., S.H. Melfi, D.N. Whiteman, and K.D. Evans, Raman lidar measurements of Pinatubo aerosols over southeastern Kansas during November-December 1991, *Geophys. Res. Lett., 19*(15), 1599–1602, 1992.

Ferrare, R.A., S.H. Melfi, D.N. Whiteman, K.D. Evans, F.J. Schmidlin and D.O'C. Starr, A Comparison of water vapor measurements made by Raman lidar and radiosondes, *J. Atmos. Oceanic Technol., 12*, 1177–1195, 1995.

Ferrare, R.A., G. Schwemmer, S.H. Melfi, K.D. Evans, D.N. Whiteman, Y.J. Kaufman, D. Guerra, and D. Wooten, Scanning Raman Lidar measurements of aerosol backscatter and extinction profiles during TARFOX, *EoS Trans. AGU, 78*(17), S81, 1997.

Ferrare, R.A., S.H. Melfi, D.N. Whiteman, K.D. Evans, M. Poellot, and Y.J. Kaufman, Raman lidar measurements of aerosol extinction and backscattering, 2, Derivation of aerosol real refractive index, single-scattering albedo, and humidification factor using Raman lidar and aircraft size distribution measurements, *J. Geophys. Res.*, this issue.

Goldsmith, J.E.M., S.E. Bisson, and F.H. Blair, Raman lidar installed at the southern Great Plains cloud and radiation testbed site for profiling atmospheric water vapor, aerosols, and clouds, paper presented at the Sixth Atmospheric Radiation Science Team Meeting, Department of Energy, San Antonio, Tex., 1996.

Halthore, R., T.F. Eck, B.N. Holben, and B.L. Markham, Sun photometric measurements of atmospheric water vapor column abundance in the 940-nm band, *J. Geophys. Res., 102*, 4343–4352, 1996.

Heintzenberg, J. and R.J. Charlson, Design and applications of the integrating nephelometer: A review, *J. Atmos. Oceanic Technol., 13*, 987–1000, 1996.

Holben, B.N., T.F. Eck, I.Slutsker, D. Tanre, J.P. Buis, A. Setzer, E. Vermote, J.A. Reagan, and Y.J. Kaufman, Multi-band automatic Sun and sky scanning radiometer for measurement of aerosols, paper presented at the Sixth International Symposium on Physical Measurement and Signatures in Remote Sensing, Ministere de l'Enseignement Superieur et de la Recherche, Val D'Isere, France, January 17–21, 1994.

Holben, B.N., et al., AERONET-A, A federated instrument network and data archive for aerosol characterization, *Remote Sens. of Environ.*, in press, 1998.

Jager, H., T. Deshler, F. Homburg, and V. Freundenthaler, Five years of lidar observations of the Pinatubo eruption cloud, in *Advances in Atmospheric Remote Sensing With Lidar*, pp. 485–488, Springer-Verlag, New York, 1997.

Kaiser, J.F., and W.A. Reed, Data smoothing using low-pass digital filters., *Rev. Sci. Instrum., 48*, 1447–1457, 1977.

Kaufman, Y.J., T.W. Brakke, and E. Eloranta, Field experiment for measurement of the radiative characteristics of a hazy atmosphere, *J. Atmos. Sci., 43*(11), 1135–1151, 1986.

Kilsby, C.G., and M.H. Smith, Comparisons of the physical and optical properties of atmospheric aerosol from airborne and surface measurements on the east coast of England, *Atmos. Environ., 21*(10), 2233–2246, 1987.

Klett, J.D., Stable analytical inversion solution for processing lidar returns, *Appl. Opt., 20*, 211–220, 1981.

Knuteson, R.O., B.A. Whitney, H.E. Revercomb, F.A. Best, and W.L. Smith, Atmospheric emitted radiance interferometer (AERI), II, Atmospheric aerosols and water vapor, paper presented at the Sixth Atmospheric Radiation Measurement (ARM) Science Team Meeting, Department of Energy, San Antonio, Tex., 1996.

Leifer, R., B. Albert, H.N. Lee, R.H. Knuth, S.F. Guggenheim, and L. Kromidas, Aerosol measurements at 60 m during the April 1994 remote cloud study intensive operating period (RCS/IOP), paper presented at the Fifth Atmospheric Radiation Measurement (ARM) Science Team Meeting, Department of Energy, San Antonio, Tex., 1995a.

Leifer, R., R.H. Knuth, S.F. Guggenheim, and B. Albert, Aerosol measurements at the Southern Great Plains site: Design and surface installation, paper presented at the Fifth Atmospheric Radiation Measurement (ARM) Science Team Meeting, San Antonio, Tex., 1995b.

Melfi, S.H., R.A. Ferrare, K.D. Evans, B. Demoz, G. Schwemmer, D. Whiteman, D. O'C. Starr, and R.G. Ellingson, Scanning Raman Lidar measurements of water vapor and aerosols during TARFOX and the water vapor IOP, paper presented at the Seventh ARM Science Team Meeting, Department of Energy, San Antonio, Tex., March 3–7, 1997.

Reagan, J.A., M.P. McCormick, and J.D. Spinhirne, Lidar sensing of aerosols and clouds in the troposphere and stratosphere, *Proc. IEEE, 77*(3), 433–448, 1989.

Remer, L., S. Gasso, D. Hegg, Y. Kaufman, and B. Holben, Urban/industrial aerosol: Ground-based Sun/sky radiometer and airborne in situ measurements, *J. Geophys. Res., 102*, 16,849–16,859, 1997.

Rosen, J.M., R.G. Pinnick, and D.M. Garvey, Measurement of extinction-to-backscatter ratio for near-surface aerosols, *J. Geophys. Res., 102*, 6017–6024, 1997.

Smith, W.L. W.F. Feltz, R.O. Knuteson, and H. E. Revercomb, PBL sounding and cloud emittance observations with ARM-CART AERI observations, paper presented at the Fifth Atmospheric Radiation Measurement (ARM) Science Team Meeting, Department of Energy, San Antonio, Tex., 1995.

Spinhirne, J.D., J.A. Reagan, and B.M. Herman, Vertical distribution of aerosol extinction cross section and inference of aerosol imaginary index in the troposphere by lidar technique, *J. Appl. Meteorol., 19*, 426–438, 1980.

Stull, R. B., *An Introduction to Boundary Layer Meteorology*, 666 pp., Kluwer Academic, Norwell, Mass., 1988.

Takamura, T., and Y. Sasano, Aerosol optical properties inferred from simultaneous lidar, aerosol-counter, and Sun photometer measurements, *J. Meteorol. Soc. Jpn., 68*(6), 729–739, 1990.

Takamura, T., Y. Sasano, and T. Hayasaka, Tropospheric aerosol optical properties derived from lidar, Sun photometer, and optical particle counter measurements, *Appl. Opt., 33*(30), 7132–7140, 1994.

Waggoner, A.P., R. E. Weiss, N.C. Ahlquist, D.S. Covert, S. Will, and R.J. Charlson, Optical characteristics of atmospheric aerosols, *Atmos. Environ., 15*, 1891–1909, 1981.

Wandinger, U., A. Ansmann, J. Reichardt, and T. Deshler, Determination of stratospheric aerosol microphysical properties from independent extinction and backscattering measurements with a Raman lidar, *Appl. Opt., 34*, 8315–8329, 1995.

R.A. Ferrare, NASA Langley Research Center, Mail Stop 401A, Bldg. 1250, Room 132A, 21 Langley Blvd., Hampton, VA 23681. (e-mail: r.ferrare@larc.nasa.gov)

S.H. Melfi, Dept. of Physics, University of Maryland Baltimore County, Baltimore, MD 21250.

D.N. Whiteman, NASA Goddard Space Flight Center, Greenbelt, MD 20771.

K.D. Evans, Joint Center for Earth Systems Technology, University of Maryland Baltimore County, Baltimore, MD 21250.

R. Leifer, Environmental Measurements Laboratory, Dept. of Energy, New York, NY 10014.

(Received December 27, 1997; revised April 13, 1998; accepted May 5, 1998.)